

Elastic electromagnetic form factors of ${}^6\text{Li}$ from three-body models

A. Eskandarian,* D. R. Lehman, and W. C. Parke

Department of Physics, The George Washington University, Washington, D.C. 20052

(Received 26 May 1988; revised manuscript received 26 July 1988)

Within the context of three-body (alpha particle plus two nucleons) models of ${}^6\text{Li}$, the ground-state longitudinal ($C0, C2$) and transverse ($M1$) electromagnetic form factors of the ${}^6\text{Li}$ nucleus are calculated. In the zero-momentum-transfer limit of the $C0$ and $M1$ form factors, the charge radius and the magnetic moment of ${}^6\text{Li}$ are extracted, respectively. An attempt is made to extract the ${}^6\text{Li}$ electric-quadrupole moment from the threshold behavior of the $C2$ form factor. By projecting the alpha-deuteron component from the three-body wave function, the contribution and role of this part of the wave function is ascertained for the elastic form factors. The Pauli exclusion principle between the alpha particle and either nucleon is found to be responsible for the minima in the form factors. With the exception of the quadrupole (only for high q values) form factor, the particular representation of the Pauli repulsion between the alpha-particle and nucleon in the $S_{1/2}$ partial wave of the interaction is unimportant. The presence of the nucleon-nucleon tensor force suppresses the values of the form factors at high q .

I. INTRODUCTION

Many properties of the $A=6$ nuclei at low excitation energies ($\lesssim 15$ MeV) can be satisfactorily explained within the framework of three-body models. In these models, the nucleus is composed of an alpha particle and two nucleons which are all treated as elementary particles. Calculations with three-body models based on non-local separable interactions between the constituent particles have been successful in explaining a number of $A=6$ phenomena, e.g., ${}^6\text{Li} \rightarrow \alpha + d$ momentum distribution,¹ ${}^6\text{Li} \rightarrow \alpha + d$ asymptotic normalization constants,^{1,2} ${}^6\text{He}$ β decay,³ the ${}^6\text{Li} \rightarrow p + (n\alpha)$ spectral function,⁴ and both elastic and inelastic $d + \alpha$ scattering.⁵⁻⁷ Moreover, such a three-body model is unambiguous in its dynamics and has no center-of-mass problem which comes with harmonic-oscillator shell-model states. Another important point: Once the parameters of the model are determined at the two-body level, no further parametrization follows and all the results obtained thereafter are direct predictions of the model. Lehman, Rai, and Ghovanlou (LRG) derived the nonrelativistic ground-state wave function of the ${}^6\text{Li}$ nucleus, using nonlocal separable potentials for the interactions between the constituent particles.⁸ Having the LRG wave function for ${}^6\text{Li}$ available to us, and encouraged by the general success of the three-body models, we undertook the calculation of the elastic electromagnetic form factors of ${}^6\text{Li}$ with the following goals in mind: (1) to explain the physics behind the observed diffraction minima in the charge and magnetic form factors, and, in particular, assess the role of the underlying two-body interactions (αN and NN) on the elastic form factors, and (2) to set a benchmark for further, more sophisticated, consistent nonrelativistic calculations. Before presenting the details of this work, we briefly review the existing literature on the subject.

Good experimental data of the past decade^{9,10} have prompted several calculations of the elastic form factors of ${}^6\text{Li}$. These calculations utilize a variety of methods

based on different models; for example, shell-model calculations (Payne and Nigam,¹¹ Bouten *et al.*¹²), resonating-group method calculations (Kanada, Kaneko, and Tang¹³), and phenomenological α - d (alpha-deuteron) cluster models (Bergstrom,¹⁴ Noble,¹⁵ Jain and Sarma,¹⁶ Merchant and Rowley¹⁷). Notable among the more sophisticated recent calculations that are closer in their goals to the spirit of the present calculation and thus more relevant to it are the cluster-model calculations of Mertelmeir and Hofmann,¹⁸ the three-body coordinate space calculations of Bang and Gignoux,¹⁹ and the three-body model calculations of Kukulini, Krasnopol'ski, Voronchev, and Sazanov in which variational techniques are employed.²⁰

Mertelmeir and Hofmann attempted a consistent cluster model description of the electromagnetic properties of the lithium and beryllium nuclei.¹⁸ The monopole and quadrupole charge form factors, and the charge radius and quadrupole moment $Q_{({}^6\text{Li})}$ of ${}^6\text{Li}$ were calculated. The monopole charge form factor is in good agreement with experiment for q (momentum-transfer) values on the first lobe before the diffraction minimum; however, in the region of the secondary maximum, the calculation underestimates the experimental data and the contribution of the quadrupole form factor becomes important. The charge radius of 2.40 fm, although smaller than the experimental value is in close agreement with the three-body calculation of Bang and Gignoux.¹⁹ Their interesting conclusion about $Q_{({}^6\text{Li})}$ was that a pure two-body (α - d) wave function was incapable of producing the small negative value of the quadrupole moment and that they had to use a three-body (αnp) wave function with s - and d -partial waves between the clusters and within the deuteron, before they could get a small negative value for $Q_{({}^6\text{Li})}$ from their calculation. This corroborates the conclusion of Merchant and Rowley.¹⁷ Mertelmeir and Hofmann's quoted value for $Q_{({}^6\text{Li})}$ is -0.076 fm² in reasonable agreement with the experimental value of

$-0.0644 \pm 0.0007 \text{ fm}^2$.²¹

Bang and Gignoux¹⁹ were the first to consider the charge form factor within the framework of three-body dynamics. Their three-body model of ${}^6\text{Li}$ utilized the NN (nucleon-nucleon) local potentials of Malfliet and Tjon,²² and of de Tourreil and Sprung's potential²³ when the tensor force was included. For the αN (alpha-nucleon) interaction an energy independent potential of the same type as that of Satchler *et al.*²⁴ was used. This αN interaction supports a bound state which is forbidden by Pauli's exclusion principle and should be removed from the problem. The Faddeev equations for the three-body problem were then solved in configuration space. The Pauli principle inclusion in the αN interaction was approximate, in the sense that the forbidden state was not eliminated from the problem completely. The monopole piece of the charge form factor was then calculated for low q values (before the diffraction minimum), and the charge radius was computed for both choices of the above NN potentials. The charge form factor is in reasonable agreement with experiment at low-momentum transfer, and the charge radius for both cases of the NN potentials (2.42 fm for Malfliet and Tjon's potential, 2.44 fm for de Tourreil and Sprung's potential) is about 4% smaller than the experimental value. Because of limitations imposed by computer space and time, they had to use a finite number of partial waves in the Faddeev equations. The truncation of available channels did not seem to affect the binding energy but was cited as responsible for the wrong sign and magnitude of the quadrupole moment. In the above work no attempt was made to calculate the quadrupole form factor, the elastic magnetic form factor or the magnetic moment of ${}^6\text{Li}$.

Kukulin, Krasnopol'ski, Voronchev, and Sazanov recently studied the ground-state properties of ${}^6\text{Li}$ using variational techniques on a three-body model of that nucleus, in a paper which complements their earlier work on the same subject.^{20,25-27} A multidimensional Gaussian basis was used and the basic variational parameters were initially randomized. Their model allows for the following: (a) the central and odd l NN forces, (b) the repulsive core of the NN interaction with s -, p -, and d -partial waves, (c) the central αN forces including the Coulomb interaction without using perturbation theory, and (d) the spin-orbit αN force. In order to take the Pauli principle into account in the αN interaction, a pseudo-potential scheme is used which, in essence, projects out the forbidden bound state of the αN interaction. However, the removal of the forbidden state is done numerically by letting the projection parameter approach a large value, when actually it can be taken to infinity analytically. The ground-state charge and magnetic form factors were calculated. The charge form factor has the correct shape but overestimates the q value of the minimum and is smaller than the experimental value in magnitude in the region of the secondary maximum and beyond. The calculated elastic magnetic form factor gives a good description of the experimental data up to the first minimum, but for higher values of q it grossly underestimates the available data. The value of the magnetic moment for ${}^6\text{Li}$ obtained from their approach with the Reid

soft-core potential, $\mu = 0.8563 \mu_N$,²⁸ is approximately 4% larger than the experimental value of $\mu_{\text{exp}} = 0.8220467 \mu_N$;²¹ however, their value for the electric quadrupole moment has the wrong sign and is about three times larger in magnitude than the experimental value. A surprising result is that the binding energy and the rms charge radius are both less than the corresponding experimental results. One would expect weaker binding to increase the rms radius. Such behavior may be checked using the three-body model of the present calculation.

The above considerations of the existing theoretical work show that a unified description of the static and dynamic properties of ${}^6\text{Li}$ in the elastic case is not achieved yet. Moreover, there are several interesting questions regarding the physics of the form factors which are not answered. For example, what component of the three-body model is responsible for the observed diffraction minimum? What effects do the underlying two-body interactions have on the shape or magnitude of the form factors? With regard to this last question, two specific points are of concern. Firstly, it is known that the $S_{1/2}$ component of the αN interaction can be represented by either a purely repulsive potential or an attractive potential that supports a forbidden bound state (due to Pauli's exclusion principle), which is usually projected out of the spectrum of the Schrödinger equation by a suitable projection method. Both representations of the Pauli principle, i.e., in terms of a purely repulsive or an attractive (with the forbidden state removed) potential, are in agreement with the present phase-shift data and only differ in their off-shell behavior.²⁹ One would like to know if the form-factor calculations are sensitive to these two different representations of the Pauli principle. Secondly, the role of the tensor force (in the NN interaction) on the electromagnetic form factors is not yet known. These and other questions can be consistently answered within the framework of a three-body model. To achieve this, we use the LRG wave function of ${}^6\text{Li}$ which has been previously derived.⁸ To unravel the effect of the underlying dynamics, we consider five potential models each of which by virtue of having different components of the underlying two-body interactions yields unambiguous information about the effect of the interactions on the form factors. A full explanation of these potentials will be given in Sec. III. The following calculations have been done: (1) The monopole charge form factor (F_{C0}) and the charge radius (extracted from F_{C0} , see Sec. II); (2) the quadrupole form factor (F_{C2}) and an attempt to calculate the quadrupole moment (extracted from F_{C2} , see Sec. II); and (3) the elastic magnetic form factor (F_M) (without the contribution of the convection currents) and the magnetic moment (extracted from F_M , see Sec. II). With these calculations, we intend to give a unified explanation of the elastic properties of the ${}^6\text{Li}$ nucleus based on a dynamically sound model. We will also try to point out the failures of the model and suggest further improvements or refinements. This calculation can also serve as a check for the results of other consistent three-body models of ${}^6\text{Li}$, since it is always advisable for different groups to perform calculations of this complexity.

The organization of this paper is as follows: In Sec. II, we present the derivation of the main formulas for the form factors and other quantities of interest, and specifically present the α - d projected model (projected from the full three-body wave function) and formulas for elastic form factors within that model; in Sec. III, we present the results with a discussion about the numerical accuracy; in Sec. IV, we discuss the physics learned from the results of our calculations; and finally, in Sec. V our conclusions are presented.

II. DERIVATION OF EQUATIONS

The experimental determination of the longitudinal and transverse form factors is done by comparing the

measured cross section with the predicted formula for the electron scattering process based on invariance arguments alone. In most cases, the form factors are determined from a Rosenbluth plot. Therefore, it is instructive to have a model-independent derivation of the cross section before we present our calculations of the form factors.

The one-photon exchange process constitutes the main contribution to the differential cross section of the scattering process. The requirements of relativistic covariance, together with parity, hermiticity, time-reversal symmetry, as well as current conservation, lead to the following expression for the electromagnetic current of any charged “spin-1” object made of individual nucleons:

$$j_{fi}^\mu = \frac{Ze}{V\sqrt{2\mathcal{E}_i 2\mathcal{E}_f}} \left[-P^\mu \left\{ F_{C0}(q^2) \left[S_f^* \cdot S_i + \frac{(S_f^* \cdot q)(S_i \cdot q)}{2m^2(1-q^2/4m^2)} \right] \right. \right. \\ \left. \left. + \sqrt{2}F_{C2}(q^2) \left[\frac{S_f^* \cdot S_i}{2} - \frac{3(S_f^* \cdot q)(S_i \cdot q)}{2q^2(1-q^2/4m^2)} \left[1 - \frac{q^2}{6m^2} \right] \right] \right\} \right. \\ \left. + F_M(q^2) \left[\frac{m}{2M} \right] \left[\frac{(S_f^* \cdot q)(S_i \cdot q)}{2m^2(1-q^2/4m^2)} P^\mu + S_f^{\mu*} (S_i \cdot q) - (S_f^* \cdot q) S_i^\mu \right] \right]. \quad (1)$$

In Eq. (1), Z is the number of unit charges, \mathcal{E}_i, S_i and \mathcal{E}_f, S_f are the initial and final energies and polarization vectors associated with the “spin-1” object, q^μ and P^μ are defined in terms of the initial and final four momenta of the “spin-1” object:

q^2 is the four-momentum transferred squared, m is the nucleus mass, M is the nucleon mass, and V is the plane-wave normalization volume. Using the above expression for the current, the laboratory scattering cross section is found to be:

$$\frac{d\sigma}{d\Omega_{e_f}} = \left(\frac{d\sigma}{d\Omega_{e_f}} \right)_{\text{Mott}} \left[\frac{1}{1 + \frac{2E_i}{m} \sin^2 \frac{\theta}{2}} \right] \left\{ F_{C0}^2(q^2) + F_{C2}^2(q^2) - \frac{q^2}{3m^2} \left[\frac{m}{ZM} \right]^2 \left[\frac{1}{2} + \left[1 - \frac{q^2}{4m^2} \right] \tan^2 \frac{\theta}{2} \right] F_M^2(q^2) \right\}, \quad (2)$$

where E_i is the energy of the initial electron, and θ is the angle between the incident and scattered electron directions. The Mott cross section is given by:

$$\left(\frac{d\sigma}{d\Omega_{e_f}} \right)_{\text{Mott}} = \frac{Z^2 \alpha^2 \cos^2(\theta/2)}{4E_i^2 \sin^4(\theta/2)},$$

where α is the fine-structure constant. It should be noted that a similar formula for the scattering cross section of Eq. (2) was found by Glendenning and Kramer,³⁰ and Gourdin³¹ for elastic electron-deuteron scattering, using the impulse approximation, a nonrelativistic wave function of the deuteron, and the nonrelativistic reduction of the electron-nucleon interaction. The nuclear current (as presented earlier in this section) was first derived by L. Durand³² for a deuteron vertex. However, the three form factors (the number of independent form factors for the case of the deuteron vertex was shown to be “three” by Glaser and Jaksic³³) associated with the “spin-1” object were not introduced to be in any way related to the charge, quadrupole, and magnetic moment distributions. It can be shown that in the Briet frame (that frame in

which the initial and final states of the scatterer have equal, but oppositely directed, momenta), F_{C0} , F_{C2} , and F_M are Fourier transforms of the charge, the electric quadrupole moment, and the magnetic moment distributions. It is important to note that such association of the form factors with spatial distributions of the electromagnetic quantities is frame dependent; the association should not be used in arbitrary frames.

A. Longitudinal form factors of ${}^6\text{Li}$

We use the LRG three-body model⁸ of ${}^6\text{Li}$ to find expressions for the two pieces of the longitudinal form factor that we denoted by F_{C0} and F_{C2} in the cross-section formula, Eq. (2). Since the isospin function is suppressed in the ${}^6\text{Li}$ wave function, it will also be suppressed in the expressions for the charge and the current operators in what follows below.

The charge-density operator in the three-body model of ${}^6\text{Li}$ is

$$\rho_c(\mathbf{r}, \mathbf{r}_1, \mathbf{r}_2, \mathbf{r}_3) = f_{\text{ch}}^p(\mathbf{r} - \mathbf{r}_1) + f_{\text{ch}}^n(\mathbf{r} - \mathbf{r}_2) + f_{\text{ch}}^\alpha(\mathbf{r} - \mathbf{r}_3), \quad (3)$$

where f_{ch}^p , f_{ch}^n , and f_{ch}^α give the spatial distribution of charge for particles 1, 2, and 3, respectively. Then,

$$ZF_{\text{ch}}^{6\text{Li}}(\mathbf{q}) = \int \langle {}^6\text{Li} | \rho_c(\mathbf{r}) | {}^6\text{Li} \rangle e^{i\mathbf{q}\cdot\mathbf{r}} d^3r. \quad (4)$$

In our case $Z=3$ normalizes the form factor so that at $q^2=0$ the total number of unit charges on ${}^6\text{Li}$ is recovered. Here, \mathbf{q} is the spatial part of the four-

momentum transfer q_μ . In coordinate space (with $q = |\mathbf{q}|$),

$$3F_{\text{ch}}^{6\text{Li}}(\mathbf{q}) = \int \prod_{j=1}^3 d^3r_j \Psi_{6\text{Li}}^\dagger \times [f_{\text{ch}}^p(\mathbf{r} - \mathbf{r}_1) + f_{\text{ch}}^n(\mathbf{r} - \mathbf{r}_2) + f_{\text{ch}}^\alpha(\mathbf{r} - \mathbf{r}_3)] \Psi_{6\text{Li}} e^{i\mathbf{q}\cdot\mathbf{r}} d^3r. \quad (5)$$

Introducing $\mathbf{r}' = \mathbf{r} - \mathbf{r}_j$ for $j=1,2,3$ in separate integrals,

$$3F_{\text{ch}}^{6\text{Li}}(\mathbf{q}) = \int \prod_{j=1}^3 d^3r_j \Psi_{6\text{Li}}^\dagger \left[e^{i\mathbf{q}\cdot\mathbf{r}_1} \int e^{i\mathbf{q}\cdot\mathbf{r}'} f_{\text{ch}}^p(\mathbf{r}') d^3r' + e^{i\mathbf{q}\cdot\mathbf{r}_2} \int e^{i\mathbf{q}\cdot\mathbf{r}'} f_{\text{ch}}^n(\mathbf{r}') d^3r' + e^{i\mathbf{q}\cdot\mathbf{r}_3} \int e^{i\mathbf{q}\cdot\mathbf{r}'} f_{\text{ch}}^\alpha(\mathbf{r}') d^3r' \right] \Psi_{6\text{Li}} \quad (6)$$

and defining

$$\int e^{i\mathbf{q}\cdot\mathbf{r}'} f_{\text{ch}}^j(\mathbf{r}') d^3r' = Z_j F_{\text{ch}}^j(q^2),$$

where

$$Z_1 = Z_2 = 1, \quad Z_3 = 2$$

and

$$F_{\text{ch}}^1(0) \equiv F_{\text{ch}}^p(0) = 1,$$

$$F_{\text{ch}}^2(0) \equiv F_{\text{ch}}^n(0) = 0,$$

$$F_{\text{ch}}^3(0) \equiv F_{\text{ch}}^\alpha(0) = 1,$$

one finally gets

$$3F_{\text{ch}}^{6\text{Li}}(\mathbf{q}) = \int \prod_{j=1}^3 d^3r_j \Psi_{6\text{Li}}^\dagger [e^{i\mathbf{q}\cdot\mathbf{r}_1} F_{\text{ch}}^p(q) + e^{i\mathbf{q}\cdot\mathbf{r}_2} F_{\text{ch}}^n(q) + 2e^{i\mathbf{q}\cdot\mathbf{r}_3} F_{\text{ch}}^\alpha(q)] \Psi_{6\text{Li}}. \quad (7)$$

In terms of Jacobi coordinates (see the Appendix), the above expression is given by

$$3F_{\text{ch}}^{6\text{Li}}(\mathbf{q}) = F_{\text{ch}}^p(q^2) \int \Psi_{6\text{Li}}^\dagger e^{i\mathbf{q}\cdot(\mathbf{s}/2 - 2\rho/3)} \Psi_{6\text{Li}} d^3\rho d^3s + F_{\text{ch}}^n(q^2) \int \Psi_{6\text{Li}}^\dagger e^{i\mathbf{q}\cdot(-\mathbf{s}/2 - 2\rho/3)} \Psi_{6\text{Li}} d^3\rho d^3s + 2F_{\text{ch}}^\alpha(q^2) \int \Psi_{6\text{Li}}^\dagger e^{i\mathbf{q}\cdot\rho/3} \Psi_{6\text{Li}} d^3\rho d^3s. \quad (8a)$$

Utilizing the symmetry of $\Psi_{6\text{Li}}$ under exchange of particles 1 and 2, one derives,

$$3F_{\text{ch}}^{6\text{Li}}(\mathbf{q}) = [F_{\text{ch}}^p(q^2) + F_{\text{ch}}^n(q^2)] \int \Psi_{6\text{Li}}^\dagger e^{i\mathbf{q}\cdot(\mathbf{s}/2 - 2\rho/3)} \Psi_{6\text{Li}} d^3\rho d^3s + 2F_{\text{ch}}^\alpha(q^2) \int \Psi_{6\text{Li}}^\dagger e^{i\mathbf{q}\cdot\rho/3} \Psi_{6\text{Li}} d^3\rho d^3s. \quad (8b)$$

To bring out the multipole character of the longitudinal form factor more clearly, one may expand the exponentials in each of the two integrands by using

$$e^{i\mathbf{q}\cdot\mathbf{r}} \equiv 4\pi \sum_{L, m_L} i^L j_L(qr) Y_{m_L}^{[L]\dagger}(\hat{\mathbf{r}}) Y_{m_L}^{[L]}(\hat{\mathbf{q}}), \quad (9)$$

where the contrastandard form³⁴ of the spherical harmonics is used, i.e., $Y_m^{[l]} = (-i^l) Y_{lm}$. The recoupling of $Y_{m_L}^{[L]}(\hat{\mathbf{r}})$ with the wave functions under the integrals eliminates all terms except those with $L=0, 1$, and 2 . The $L=1$ term vanishes because of its negative parity (the ground state of ${}^6\text{Li}$ has positive parity). Then the longitudinal form factor is given by

$$\begin{aligned}
F_{\text{ch}}^{6\text{Li}}(\mathbf{q}) = \frac{1}{3} \left\{ [F_{\text{ch}}^p(q^2) + F_{\text{ch}}^n(q^2)] \int \Psi_{M_f}^{[1]\dagger} j_0(qr_1) \Psi_{M_i}^{[1]} d^3\rho d^3s \right. \\
\left. + 2F_{\text{ch}}^\alpha(q^2) \int \Psi_{M_f}^{[1]\dagger} j_0(qr_3) \Psi_{M_i}^{[1]} d^3\rho d^3s \right\} \\
- \frac{4\pi}{3} \sum_{M_L} Y_{M_L}^{[2]\dagger}(\hat{\mathbf{q}}) \left\{ [F_{\text{ch}}^p(q^2) + F_{\text{ch}}^n(q^2)] \int \Psi_{M_f}^{[1]\dagger} j_2(qr_1) Y_{M_L}^{[2]}(\hat{\mathbf{r}}_1) \Psi_{M_i}^{[1]} d^3\rho d^3s \right. \\
\left. + 2F_{\text{ch}}^\alpha(q^2) \int \Psi_{M_f}^{[1]\dagger} j_2(qr_3) Y_{M_L}^{[2]}(\hat{\mathbf{r}}_3) \Psi_{M_i}^{[1]} d^3\rho d^3s \right\}, \quad (10)
\end{aligned}$$

where the total angular momentum of the ground-state wave function of ${}^6\text{Li}(J^\pi=1^+)$ is now explicit, but the subscript (${}^6\text{Li}$) is omitted. By the use of the Wigner-Eckart theorem, the above expression may be simplified further, and written in terms of invariant integrals:

$$F_{\text{ch}}^{6\text{Li}}(\mathbf{q}) = F_{C_0}(q^2) \delta_{M_f, M_i} + \sqrt{12\pi} F_{C_2}(q^2) \sum_{m_L} (-1)^{1+M_i} \begin{pmatrix} 1 & 1 & 2 \\ -M_f & M_i & m_L \end{pmatrix} Y_{m_L}^{[2]\dagger}(\hat{\mathbf{q}}), \quad (11)$$

where

$$\begin{pmatrix} 1 & 1 & 2 \\ -M_f & M_i & m_L \end{pmatrix}$$

is a 3- j symbol; $F_{C_0}(q^2)$ and $F_{C_2}(q^2)$ in momentum space are

$$\begin{aligned}
F_{C_0}(q^2) = \frac{1}{12\pi\sqrt{3}} \{ [F_{\text{ch}}^p(q^2) + F_{\text{ch}}^n(q^2)] [\tilde{\psi}^{[1]}(\mathbf{p}, \mathbf{k}) | \Psi^{[1]}(\mathbf{p} + 2\mathbf{q}/3, \mathbf{k} - \mathbf{q}/2)] \\
+ 2F_{\text{ch}}^\alpha(q^2) [\tilde{\psi}^{[1]}(\mathbf{p}, \mathbf{k}) | \Psi^{[1]}(\mathbf{p} - \mathbf{q}/3, \mathbf{k})] \}, \quad (12)
\end{aligned}$$

$$\begin{aligned}
F_{C_2}(q^2) = \frac{1}{12\pi\sqrt{3}} \{ [F_{\text{ch}}^p(q^2) + F_{\text{ch}}^n(q^2)] [\tilde{\Psi}^{[1]}(\mathbf{p}, \mathbf{k}) | Y^{[2]}(\hat{\mathbf{q}}) | \Psi^{[1]}(\mathbf{p} + 2\mathbf{q}/3, \mathbf{k} - \mathbf{q}/2)] \\
+ 2F_{\text{ch}}^\alpha(q^2) [\tilde{\Psi}^{[1]}(\mathbf{p}, \mathbf{k}) | Y^{[2]}(\hat{\mathbf{q}}) | \Psi^{[1]}(\mathbf{p} - \mathbf{q}/3, \mathbf{k})] \}, \quad (13)
\end{aligned}$$

where, for instance,

$$\begin{aligned}
\int \Psi_{M_f}^{[1]\dagger}(\mathbf{p}, \mathbf{k}) Y_{m_L}^{[2]}(\hat{\mathbf{q}}) \Psi_{M_i}^{[1]}(\mathbf{p} + 2\mathbf{q}/3, \mathbf{k} - \mathbf{q}/2) d^3p d^3k d\Omega_q \\
= (-1)^{1+M_f} \begin{pmatrix} 1 & 2 & 1 \\ -M_f & m_L & M_i \end{pmatrix} [\tilde{\Psi}^{[1]}(\mathbf{p}, \mathbf{k}) | Y^{[2]}(\hat{\mathbf{q}}) | \Psi^{[1]}(\mathbf{p} + 2\mathbf{q}/3, \mathbf{k} - \mathbf{q}/2)]. \quad (14)
\end{aligned}$$

In all the above formulas the notation of Ref. 34 is used for angular momenta, tensor operators, and invariant integrals. The projection integral $[\dots | \dots | \dots]$ is different from the reduced matrix element by only a phase factor and implies that all the spin sums, radial, and angular integrations are done. Now, it is easily checked that

$$\frac{1}{3} \sum_{M_i, M_f} |F_{\text{ch}}^{6\text{Li}}(\mathbf{q})|^2 = |F_{C_0}(q^2)|^2 + |F_{C_2}(q^2)|^2. \quad (15)$$

Corresponding to a well-known result for a ‘‘spin-0’’ form factor, one may also find an expression for the root-mean-squared charge radius of ${}^6\text{Li}$:

$$\langle r_{\text{ch}}^2 \rangle^{6\text{Li}} = -6 \left. \frac{\partial F_{C_0}(q^2)}{\partial q^2} \right|_{q=0}.$$

Similar formulas apply to the proton and alpha particles, but

$$\langle r_{\text{ch}}^2 \rangle^n \equiv 0. \quad (16)$$

In this work, the root-mean-squared charge radius of ${}^6\text{Li}$ is extracted from $F_{C_0}(q^2)$ by finding the slope of $F_{C_0}(q^2)$ around the origin. On the other hand, the behavior of $F_{C_2}(q^2)$ as $q^2 \rightarrow 0$ yields a quantity that is proportional to $Q_{6\text{Li}}$. The quadrupole moment can be found using

$$Q = \langle Jm_J = J | (\sqrt{16\pi/5}) \sum_{i=1}^{N_c} e_i^c r_i^2 Y_{20}(\hat{\mathbf{r}}_i) | Jm_J = J \rangle, \quad (17)$$

where e_i^c is the number of unit charges in the cluster C and N_c is the number of clusters. By taking the limit of the expression for $F_{C_2}(q^2)$ as $q^2 \rightarrow 0$, it follows that

$$\left. \frac{\partial F_{C_2}(q^2)}{\partial q^2} \right|_{q^2=0} = \frac{1}{9\sqrt{2}} Q_{6\text{Li}}. \quad (18)$$

This expression shows that, in principle, the electric quadrupole moment, like the rms radius, may be extracted by finding the slope of the $F_{C2}(q^2)$ vs q^2 plot near the origin.

B. Transverse (magnetic) form factor

To derive the expression for the elastic transverse form factor, the transverse projection of the current operator is needed. By the minimal coupling of the electromagnetic field in the nonrelativistic Hamiltonian of the three-body model, and noting that the Hamiltonian interaction is proportional to the dot product of the field and the current, the expression for the nucleus current is extracted. After some simplifications in the form of the operator, the transverse part of it may be written as

$$\hat{\epsilon}_\lambda \cdot \mathbf{J} = i \sum_{j=1}^3 e^{i\mathbf{q} \cdot \mathbf{r}_j} \left[e_j F_{\text{ch}}^j(q^2) \frac{P_{j\lambda}^{[1]}}{M_j} + \bar{\delta}_{3j} \frac{F_{\text{mag}}^j(q^2)}{2M_j} \mu_j q \lambda \sigma_{j\lambda}^{[1]} \right]. \quad (19)$$

In Eq. (19), $F_{\text{ch}}^j(q^2)$ for $j=1,2,3$ (i.e., p , n , and α , respectively) is the constituent particle's charge form factor, $F_{\text{mag}}^j(q^2)$ for $j=1,2$ is the magnetic form factor of the proton and neutron, respectively, e_j is the charge of each constituent particle, and M_j is the corresponding mass with $M_1=M_2$. $\hat{\epsilon}_\lambda$ is a unit polarization vector of the exchanged virtual photon, and $\lambda (= \pm 1)$ designates one of the two possible independent polarization directions in the plane. The operators are written in the contrastandard notation,³⁴ for example, $P_{j\lambda}^{[1]}$ is the λ component of the momentum of the j th particle. μ_j is the magnetic moment of the j th particle,

$$F_{\text{mag}}^j(0) = 1, \quad (20)$$

and

$$\bar{\delta}_{3j} \equiv (1 - \delta_{3j}). \quad (21)$$

The matrix element of the above operator is given by

$$\langle f | \hat{\epsilon}_\lambda \cdot \mathbf{J} | i \rangle = i \sum_{j=1}^3 \int \Psi_{M_f}^{[1]\dagger} e^{i\mathbf{q} \cdot \mathbf{r}_i} \left[e_j F_{\text{ch}}^j(q^2) \frac{P_{j\lambda}^{[1]}}{M_j} + \bar{\delta}_{3j} \mu_j q \lambda \frac{F_{\text{mag}}^j(q^2)}{2M_j} \sigma_{j\lambda}^{[1]} \right] \Psi_{M_i}^{[1]} d^3\rho d^3s, \quad (22)$$

where $M_j = M$ for $j=1,2$. This matrix element in the limit of $q \rightarrow 0$ is proportional to the magnetic moment of ${}^6\text{Li}$. The magnetic moment operator is

$$\mu_\lambda^{[1]} \equiv \sum_{j=1}^3 \left[\left(\frac{1}{2}\right) L_{j\lambda}^{[1]} + \bar{\delta}_{3j} \mu_j \sigma_{j\lambda}^{[1]} \right], \quad (23)$$

where L_j represents the angular momentum of the j th particle. Using the above, one finds that

$$\mu_{6\text{Li}} = \frac{-i}{\sqrt{6}} [\tilde{\Psi}^{[1]} | \mu^{[1]} | \Psi^{[1]}] \quad (24)$$

in the notation of invariant integrals. We use this proportionality of the matrix element in Eq. (22) and the magnetic moment, Eq. (24), in the limit of $q \rightarrow 0$ to normalize the magnetic form factor of ${}^6\text{Li}$ such that

$$F_M^{6\text{Li}}(0) = \mu_{6\text{Li}}. \quad (25)$$

As in the case of the charge form factor, the plane-wave exponential in the expression for the matrix element, Eq. (22), may be expanded. The recoupling of the terms in the expansion, using considerations of rotational, parity and time-reversal invariance, forces most of the terms to vanish. Application of the Wigner-Eckart theorem on the surviving terms, and expressing them in terms of the invariant integrals results in the final expression for $F_M(q^2)$ in momentum space:

$$\begin{aligned} F_M(q^2) = & \frac{-i}{\sqrt{4\pi}\sqrt{6}} (e [F_{\text{ch}}^p(q^2) + F_{\text{ch}}^n(q^2)] (-i\sqrt{6}) \\ & \times [\tilde{\Psi}^{[1]}(\mathbf{p}, \mathbf{k}) | [Y^{[1]}(\hat{\mathbf{q}}) \times P^{[1]}]^{[1]} | \Psi^{[1]}(\mathbf{p} + 2\mathbf{q}/3, \mathbf{k} - \mathbf{q}/2)] \\ & + (-i\sqrt{3/2}) e F_{\text{ch}}^\alpha(q^2) [\tilde{\Psi}(\mathbf{p}, \mathbf{k}) | [Y^{[1]}(\hat{\mathbf{q}}) \times P^{[1]}]^{[1]} | \Psi^{[1]}(\mathbf{p} - \mathbf{q}/3, \mathbf{k})] \\ & + [\mu_p F_{\text{mag}}^p(q^2) + \mu_n F_{\text{mag}}^n(q^2)]) \\ & \times ([\tilde{\Psi}^{[1]}(\mathbf{p}, \mathbf{k}) | [Y^{[0]} \times \sigma^{[1]}]^{[1]} | \Psi^{[1]}(\mathbf{p} + 2\mathbf{q}/3, \mathbf{k} - \mathbf{q}/2)] \\ & - (1/\sqrt{2}) [\tilde{\Psi}^{[1]}(\mathbf{p}, \mathbf{k}) | [Y^{[2]}(\hat{\mathbf{q}}) \times \sigma^{[1]}]^{[1]} | \Psi^{[1]}(\mathbf{p} + 2\mathbf{q}/3, \mathbf{k} - \mathbf{q}/2)]). \end{aligned} \quad (26)$$

In the actual calculations, we only consider the spin-current terms in the above expression; the convection contribution is neglected due to its complexity relative to the size of its contribution compared to the spin current.

In any calculation of form factors, the question of the importance of the mesonic degrees of freedom is raised. How significant are the meson exchange currents in a calculation like this one? The lowest-order contribution of the isoscalar meson exchange current to the charge operator is a relativistic correction of $O(v^2/c^2)$ or equivalently $O(1/M^2)$.^{35,36} The LRG wave function is nonrelativistic and of order $O(1)$. To include relativistic corrections in such calculations, the wave function should also be corrected to $O(1/M^2)$ for consistent results. Any attempt to include the $O(1/M^2)$ meson exchange corrections with the available wave function would be inconsistent, and yield ambiguous results. The same situation prevails in the case of the elastic magnetic form fac-

tors where the lowest-order mesonic contributions are of $O(1/M^3)$, and should not be included in a consistent calculation of the magnetic form factor unless relativistic corrections are also accounted for in the wave functions to the same order.

C. Elastic form factors from the projected α - d component

We give the derivation of the elastic form factors of ${}^6\text{Li}$ in a two-body (αd) model in which a real deuteron wave function and an elementary α particle are projected from the three-body (αnp) model of ${}^6\text{Li}$. This enables one to distinguish the contributions of the α -(np) component (three-body correlations) in the results. To achieve this, we use the completeness of plane waves and the two-nucleon states in Eq. (8b).

Specifically, for the two nucleons,

$$\sum_{m_d} \varphi_{m_d}^{[1]}(\mathbf{s}) \varphi_{m_d}^{[1]\dagger}(\mathbf{s}') + \text{scattering contribution} = \delta^3(\mathbf{s} - \mathbf{s}'), \quad (27)$$

where $\varphi_{m_d}^{[1]}(\mathbf{s})$ is the deuteron wave function in coordinate space. If the ‘‘scattering contribution’’ to the completeness relationship in Eq. (27) is ignored, one obtains $F_{\text{ch}}^{6\text{Li}}(\mathbf{q})$ in the α - d model. Then the form factor may be written as

$$3F_{\text{ch}}^{6\text{Li}}(\mathbf{q}) = [F_{\text{ch}}^p(q^2) + F_{\text{ch}}^n(q^2)] I_1^{\alpha d} + 2F_{\text{ch}}^\alpha(q^2) I_2^{\alpha d}, \quad (28)$$

where

$$I_1^{\alpha d} = \sum_{m_d} \int d^3 Q \int d^3 \rho d^3 s e^{-i\mathbf{q}\cdot(2/3)\rho} \frac{e^{i\mathbf{Q}\cdot\rho}}{(2\pi)^{3/2}} \Psi_m^{[1]\dagger}(\rho, \mathbf{s}) \varphi_{m_d}^{[1]}(\mathbf{s}) \\ \times \int d^3 s' e^{i(\mathbf{q}/2)\cdot\mathbf{s}'} \varphi_{m_d}^{[1]\dagger}(\mathbf{s}') \varphi_{m_d}^{[1]}(\mathbf{s}') \int d^3 \rho' d^3 s'' \frac{e^{-i\mathbf{Q}\cdot\rho'}}{(2\pi)^{3/2}} \varphi_{m_d}^{[1]\dagger}(\mathbf{s}'') \Psi_m^{[1]}(\rho', \mathbf{s}'') \quad (29)$$

and

$$I_2^{\alpha d} = \sum_{m_d} \int d^3 Q \int d^3 \rho d^3 s e^{i\mathbf{q}\cdot\rho/3} \frac{e^{i\mathbf{Q}\cdot\rho}}{(2\pi)^{3/2}} \Psi_m^{[1]\dagger}(\rho, \mathbf{s}) \varphi_{m_d}^{[1]}(\mathbf{s}) \int d^3 \rho' d^3 s' \frac{e^{-i\mathbf{Q}\cdot\rho'}}{(2\pi)^{3/2}} \varphi_{m_d}^{[1]\dagger}(\mathbf{s}') \Psi_m^{[1]}(\rho', \mathbf{s}'). \quad (30)$$

We define the alpha-deuteron overlap amplitude

$$\langle \alpha d; \mathbf{Q}, 1m'_d | {}^6\text{Li}; 1m \rangle \equiv \int d^3 \rho' d^3 s'' \frac{e^{-i\mathbf{Q}\cdot\rho'}}{(2\pi)^{3/2}} \varphi_{m_d}^{[1]\dagger}(\mathbf{s}'') \Psi_m^{[1]}(\rho', \mathbf{s}''), \quad (31)$$

then

$$I_1^{\alpha d} = \sum_{m_d, m'_d} \int d^3 s' e^{i(\mathbf{q}/2)\cdot\mathbf{s}'} \varphi_{m_d}^{[1]\dagger}(\mathbf{s}') \varphi_{m_d}^{[1]}(\mathbf{s}') \int d^3 Q \langle {}^6\text{Li}, 1m' | \alpha d; \mathbf{Q} - 2\mathbf{q}/3, 1m'_d \rangle \langle \alpha d; \mathbf{Q}, 1m_d | {}^6\text{Li}; 1m \rangle \quad (32)$$

and

$$I_2^{\alpha d} = \sum_{m_d} \int d^3 Q \langle {}^6\text{Li}; 1m' | \alpha d; \mathbf{Q} + \mathbf{q}/3, 1m_d \rangle \langle \alpha d; \mathbf{Q}, 1m_d | {}^6\text{Li}; 1m \rangle. \quad (33)$$

According to the work of Lehman and Rajan:¹

$$\langle \alpha d; \mathbf{Q}, 1m_d | {}^6\text{Li}; 1m \rangle = \sum_{l, m_l} f_l(Q) \langle lm_l 1m | 1m_d \rangle \sqrt{4\pi} Y_{m_l}^{[1]\dagger}(\hat{\mathbf{Q}}), \quad (34)$$

where $f_l(Q)$ is the l th partial-wave α - d momentum-distribution amplitude for ${}^6\text{Li}$, with $f_0(Q)$ being dominant and $f_2(Q)$ negligible compared to $f_0(Q)$ except at the zero of $f_0(Q)$. The quantum number l is even because of the positive parity of the ${}^6\text{Li}$ nucleus, and ≤ 2 due to the deuteron and ${}^6\text{Li}$ both having spin 1. It is also important to note that in

the I_1^{ad} case, the body form factor of the deuteron appears and so the deuteron's charge form factor can be defined in exactly the same way as the ${}^6\text{Li}$ charge form factor (both of them being 1^+ objects):

$$\begin{aligned} F_{\text{ch}}^d(\mathbf{q}) &= [F_{\text{ch}}^p(q^2) + F_{\text{ch}}^n(q^2)] \int d^3s' e^{i(\mathbf{q}/2)\cdot\mathbf{s}'} \varphi_{m_d}^{[1]}(\mathbf{s}')^\dagger \varphi_{m_d}^{[1]}(\mathbf{s}') \\ &\equiv F_{C_0}^d(q^2) \delta_{m_d', m_d} + \sqrt{12\pi} F_{C_2}^d(q^2) \sum_{m_k} (-1)^{1+m_d'} \begin{pmatrix} 1 & 2 & 1 \\ -m_d' & m_k & m_d \end{pmatrix} Y_{m_k}^{[2]\dagger}(\hat{\mathbf{q}}), \end{aligned} \quad (35)$$

where $F_{C_0}^d(q^2)$ and $F_{C_2}^d(q^2)$ are related to the static properties of the deuteron by:

$$\lim_{q^2 \rightarrow 0} F_{C_0}^d(q^2) = 1$$

and

$$\lim_{q^2 \rightarrow 0} F_{C_2}^d(q^2) = \frac{q^2 Q_d}{3\sqrt{2}}.$$

Q_d denotes the quadrupole moment of the deuteron. If we neglect the d -wave α - d overlap amplitude, $f_2(q)$, the ${}^6\text{Li}$ monopole charge factor has the form

$$3F_{C_0}^{6\text{Li}}(q) = F_{C_0}^d(q) \bar{I}_1^{ad} + 2F_{\text{ch}}^d(q) \bar{I}_2^{ad}, \quad (37)$$

where

$$\bar{I}_1^{ad} \equiv \int d^3Q f_0(|\mathbf{Q} - 2\mathbf{q}/3|) f_0(Q) \quad (38a)$$

and

$$\bar{I}_2^{ad} \equiv \int d^3Q f_0(|\mathbf{Q} + \mathbf{q}/3|) f_0(Q), \quad (38b)$$

while the quadrupole form factor becomes

$$3F_{C_2}^{6\text{Li}}(q) = F_{C_2}^d(q) \bar{I}_1^{ad}. \quad (39)$$

When $f_2(q)$ is not neglected, we find

$$\lim_{q \rightarrow 0} F_{C_0}^{6\text{Li}}(q) = 4\pi \int_0^\infty q'^2 dq' \{ [f_0(q)]^2 + [f_2(q)]^2 \}, \quad (40)$$

where the right-hand side is the percentage of α - d component in the three-body ${}^6\text{Li}$ wave function. In an analogous fashion, the quadrupole moment of ${}^6\text{Li}$ in the α - d projection is given by

$$\begin{aligned} Q_{6\text{Li}} &= Q_d \left\{ 4\pi \int_0^\infty \rho^2 d\rho \{ [u_0(\rho)]^2 + (\frac{1}{10}) [u_2(\rho)]^2 \} \right. \\ &\quad \left. + \frac{4\sqrt{2}}{15} \left\{ 4\pi \int_0^\infty \rho^2 d\rho \rho^2 u_2(\rho) u_0(\rho) - (4\pi/2\sqrt{2}) \int_0^\infty \rho^2 d\rho \rho^2 [u_2(\rho)]^2 \right\} \right\}, \end{aligned} \quad (41)$$

where

$$u_l(q) = \sqrt{2/\pi} \int_0^\infty q^2 dq j_l(q\rho) f_l(q). \quad (42)$$

The quadrupole moment at this level has two contributions: (1) From the intrinsic quadrupole moment of the deuteron times what is essentially the fraction of α - d component in the ${}^6\text{Li}$ wave function, and (2) from the d -wave relative motion of the alpha particle and the deuteron.

For the elastic magnetic form-factor calculation in the α - d projected model, we follow the same procedure outlined in Eqs. (27)–(33) for the matrix element:

$$\langle f | \boldsymbol{\epsilon}_\lambda \cdot \mathbf{J} | i \rangle = \frac{i q_\lambda}{2M} [\mu_p F_M^p(q^2) + \mu_n F_M^n(q^2)] \int \Psi_m^{[1]\dagger}(\boldsymbol{\rho}, \mathbf{s}) e^{i\mathbf{q}\cdot(\mathbf{s}/2 - 2\rho/3)} \sigma_{1\lambda}^{[1]} \Psi_m^{[1]}(\boldsymbol{\rho}, \mathbf{s}) d^3\rho d^3s. \quad (43)$$

Here again, if we take only the s -wave piece of the αd - ${}^6\text{Li}$ overlap amplitude, we find, after some algebra, that $F_M(q)$ is given by

$$F_M(q) = F_M^d(q) \bar{I}_1^{\alpha d}, \quad (44)$$

where $F_M^d(q)$ is the deuteron magnetic form factor.

III. RESULTS

Before the actual presentation of the results, we summarize the utility of the five two-body interaction models employed in this work. The "simple model," by having only the $P_{3/2}$ part of the αN interaction,² enables us to observe the effects of the presence of the $S_{1/2}$ interaction which is included in all the other four models.^{8,29} The $P_{1/2}$ part of the αN interaction is also included in the remaining four models, but it is weak enough that any major observable difference between the "simple model" and the other models is attributed to the presence of the $S_{1/2}$ interaction in those other models. The "full-repulsive" and "projected bound-state" models enable us to see the differences in the representation of the $S_{1/2}$ interaction in the αN system; and each of them is employed with an NN interaction that yields either (4%) or (0%) D -state probability in the deuteron so that the effect of the tensor force in the NN system can be studied.

The general procedure for the calculation of all the form factors involved in this work is as follows: First, with the ${}^6\text{Li}$ wave function as given in the Appendix,⁸ all the recouplings of the spin and angular functions are done using Danos' method;³⁴ therefore, all the spin sums are performed first, and then the angular and radial integrations are performed.

The coupling of the spherical harmonic functions to zero is expressed in terms of polynomials in scalar products of the vectors found in the arguments of those spherical harmonics involved. This method has been used in the previous works of Lehman and collaborators involving the ${}^6\text{Li}$ wave function.^{37,38} The polynomials mentioned are obtained by properly contracting all the tensors involved to yield a scalar function in terms of the angular variables. In order to check our derivations, the symbolic manipulation module REDUCE was used to program the above method. The program developed is general enough to allow for the coupling of any number of spherical harmonic functions to zero. Another REDUCE program generates a FORTRAN code of all the terms in the matrix element with their proper phases, coefficients and couplings. This FORTRAN code is then included in a bigger program which performs the numerical integrations.

The parameters for the isoscalar nucleon charge and magnetic form factors required in the calculations of the monopole and quadrupole charge form factors and the magnetic elastic form factor of ${}^6\text{Li}$ were taken from Hohler *et al.*³⁹ It is important to note here that different sets of parameters of Hohler *et al.* have different normalizations at $q=0$. For example, the different sets are not constrained to yield unity for the nucleon isoscalar

charge form factor at $q=0$. For the parametrization of the α -particle form factor, the formula of Frosch *et al.* was used.⁴⁰ The charge and magnetic form factors of the deuteron, which were used in the projected α - d (two-body) calculations of the ${}^6\text{Li}$ nucleus, were kindly provided by Friar (for the Reid soft-core potential).⁴¹

A. Monopole charge form factor

As a check of the form-factor code, the contributions of all the components of the wave function in the normalization integral, which was done earlier and with a different method of derivation⁸ were compared with those produced by the F_{C0} code at $q^2=0$ [it is easy to show that $F_{C0}(0)$ and the normalization integral are identical]. The analytical and numerical results both agreed between these two different methods for all the potential models considered here. The results for the F_{C0} form factor using different models are shown in Figs. 1–4. In Fig. 1, the result for the projected bound-state (4%) model, which is one of the best models used (because of its better prediction of the binding energy relative to other models), is plotted against the experimental data. Most models show a diffraction minimum between $q^2=9.0 \text{ fm}^{-2}$ and $q^2=10.0 \text{ fm}^{-2}$. The full-repulsive (0%) model has the minimum between $q^2=8.0 \text{ fm}^{-2}$ and $q^2=9.0 \text{ fm}^{-2}$. The simple model does not reproduce the diffraction minimum at all. In Fig. 5, the F_{C0} form factor for the projected α - d component of ${}^6\text{Li}$ is presented vs the three-body projected bound-state (4%) model of ${}^6\text{Li}$. The projected α - d predicts a minimum between $q^2=10 \text{ fm}^{-2}$ and $q^2=10.5 \text{ fm}^{-2}$. To find the charge radius of ${}^6\text{Li}$ from the F_{C0} form factor, six points are generated near the origin, and a least-squares fit is done. The slope of this line then

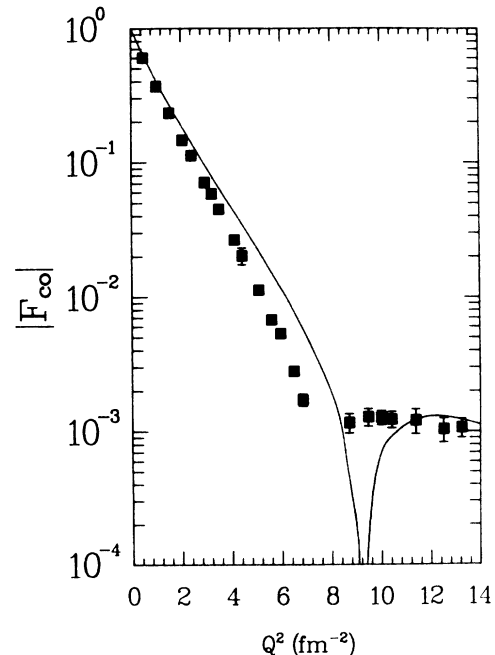


FIG. 1. The monopole charge form factor of ${}^6\text{Li}$ for the projected bound-state (4%) model, and the experimental data.

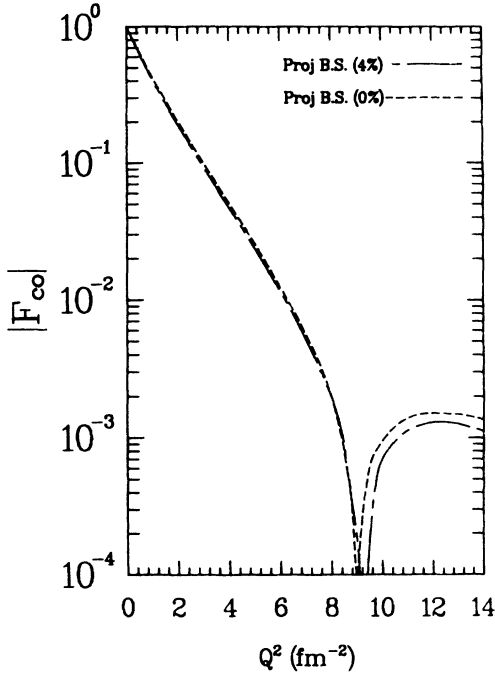


FIG. 2. The monopole charge form factor of ${}^6\text{Li}$ for the projected bound-state (4%), and projected bound-state (0%) models.

determines the charge radius. In Table I, the calculated charge radii for different models are presented next to the binding energies in the corresponding models. A linear least-squares fit to the charge radius (R_{ch}) vs the binding energy (B) for the values in Table I gives

$$R_{\text{ch}} = -(0.22 \pm 0.02)B + (3.32 \pm 0.06)$$

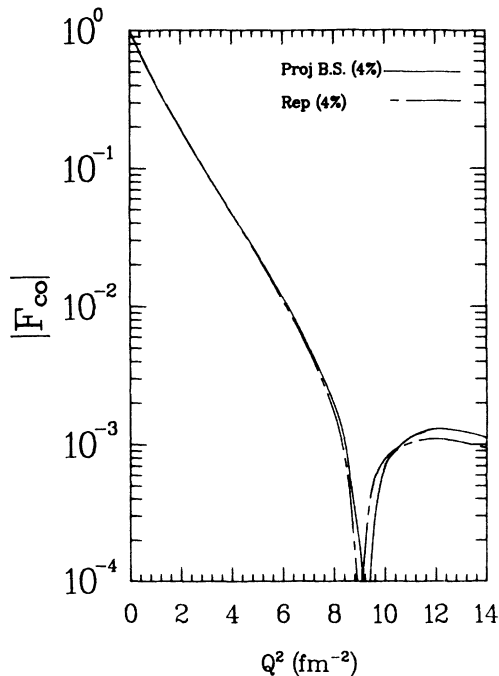


FIG. 3. The monopole form factor of ${}^6\text{Li}$ for the full-repulsive (4%), and projected bound-state (4%) models.

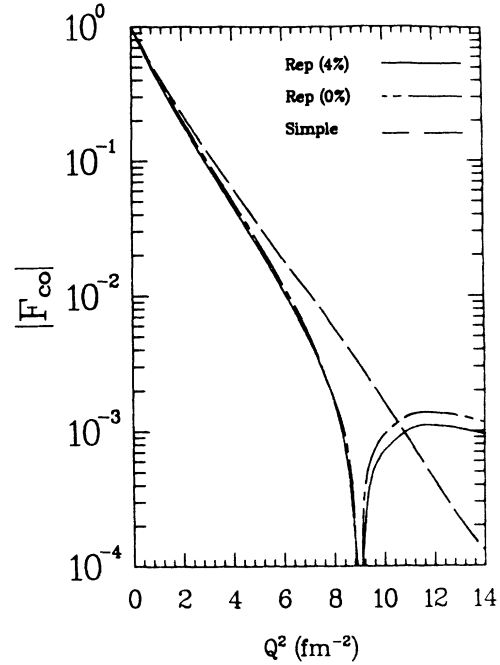


FIG. 4. The monopole charge form factor of ${}^6\text{Li}$ for the full-repulsive (4%), full-repulsive (0%), and simple models.

with correlation coefficient $r^2=0.991$.

It is found that for q^2 values up to 6.0 fm^{-2} it suffices to use 10-Gegenbauer (for two-radial integrations), 6-Gaussian (for the two-polar-angle integration), and 20-Simpson (for one-azimuthal-angle integrations) grid points for the desired accuracy of three significant figures. However, for $q^2=6.0$ up to 14.0 fm^{-2} , one must use 16-Gegenbauer, 10-Gaussian, and 20-Simpson grid points in order to get the desired accuracy.

B. Quadrupole form factor

The number of terms in the quadrupole-form-factor matrix element is considerably larger than the monopole form factor, mainly because the operator in the quadrupole

TABLE I. The electrical charge radius of ${}^6\text{Li}$. Experimental result, Ref. 1: $R_{\text{ch}, {}^6\text{Li}} = 2.56 \pm 0.05 \text{ fm}$.

Potential model	Binding energy (MeV)	Charge radius (fm)
Simple	4.6720	2.257
Repulsive (0%)	4.4460	2.325
Repulsive (4%)	4.0624	2.403
Projected bound state (0%)	4.2940	2.352
Projected bound state (4%)	3.9030	2.434

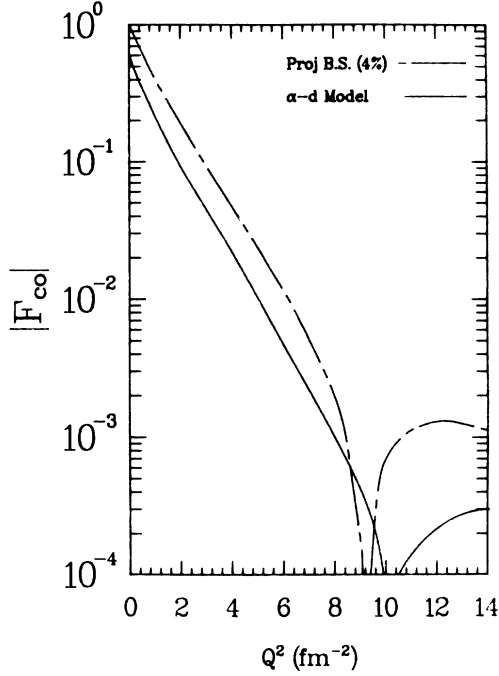


FIG. 5. The monopole form factor of ${}^6\text{Li}$ for the three-body and two-body (α - d) projected bound-state (4%) models.

pole case is of rank two and allows for more angular momentum couplings between the different components of the ground-state wave function. Therefore, the angular dependence of the form factor is also more complicated than the monopole case. This makes the numerical extraction of the quadrupole moment of ${}^6\text{Li}$ from the low q^2 behavior of the form factor very difficult. The extraction of the quadrupole moment was attempted here, using Eq. (18) and noting that

$$Q_{6\text{Li}} = (1/9\sqrt{2}) \lim_{q^2 \rightarrow 0} \frac{F_{C2}(q^2)}{q^2}.$$

The attempt was unsuccessful because the numerical integration of the complicated integrand of F_{C2} is not accurate enough to allow for a stable value of the ratio $[F_{C2}(q^2)/q^2]$ for low- q^2 values. The accuracy of results for this limit were checked for different integration grid points. Even with 24-Gegenbauer, 16-Gaussian, and 40-Simpson grid points stability was not reached. The cost for any checks beyond the above becomes prohibitive.

For the plot of the F_{C2} form factor, the 16-Gegenbauer, 10-Gaussian, 20-Simpson integration grid point scheme yields adequately accurate results for higher q^2 values. In Fig. 6 a plot of the absolute value of the charge form factor of ${}^6\text{Li}$ is given with explicit separation of the monopole and quadrupole contributions [note that $(F_{\text{ch}}^{6\text{Li}})^2 = F_{C0}^2 + F_{C2}^2$]. Figures 7–9 show the F_{C2} form factor for different models. In all models a maximum is reached between $q^2 = 1.0 \text{ fm}^{-2}$ and $q^2 = 1.5 \text{ fm}^{-2}$. Then the form factor drops without any further structure for higher q^2 values. In this work, the charge form factor of ${}^6\text{Li}$ and its rms charge radius are compared with the experimental results of Li *et al.*⁹ (Figs. 1 and 6).

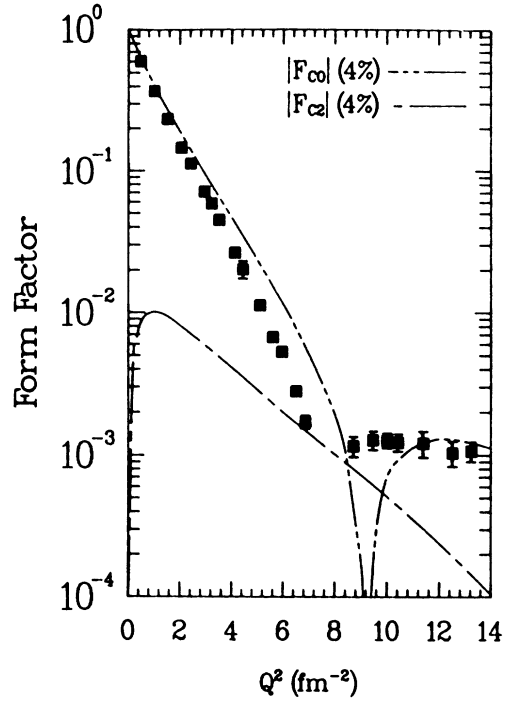


FIG. 6. The total charge form factor of ${}^6\text{Li}$ for the projected bound-state (4%) model, with the monopole and quadrupole contributions separated, and the experimental data.

C. Elastic magnetic form factor

In the calculation of the magnetic form factor, the convection contributions to the current operator were neglected for the reason given in Sec. II. Even the spin part of the current operator is not fully included. All the terms for the $[\sigma^{[1]} \times Y^{[0]}(\hat{q})]^{[1]}$ operator, and only the

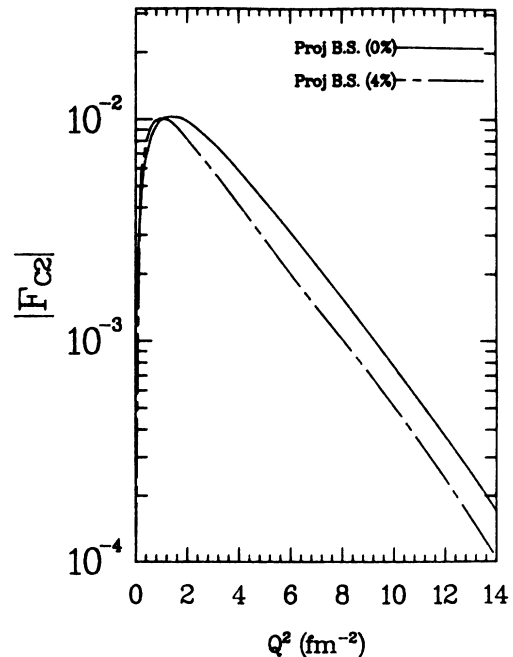


FIG. 7. The quadrupole form factor of ${}^6\text{Li}$ for the projected bound-state (4%) and projected bound-state (0%) models.

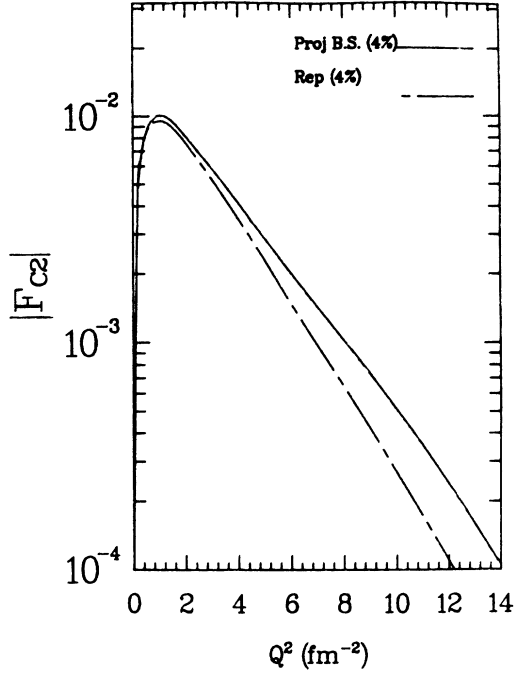


FIG. 8. The quadrupole form factor of ${}^6\text{Li}$ for the projected bound-state (4%) and the full-repulsive (4%) models.

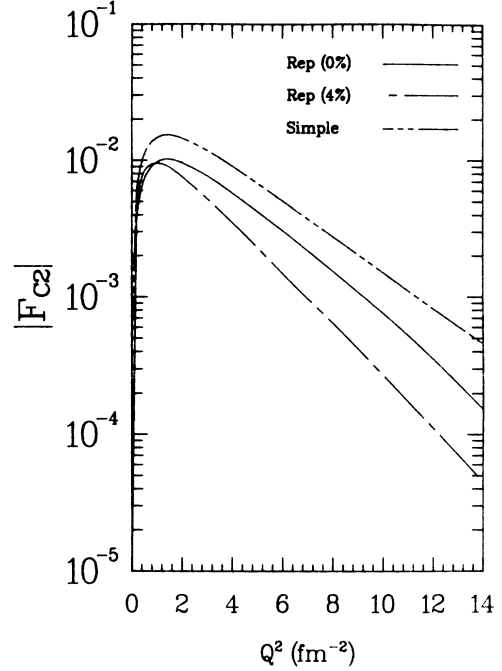


FIG. 9. The quadrupole form factor of ${}^6\text{Li}$ for the full-repulsive (4%), full-repulsive (0%), and the simple models.

most important contributions of the $[\sigma^{[1]} \times Y^{[2]}(\hat{q})]^{[1]}$ are in the final results. The inclusion of only the important terms for the $[\sigma^{[1]} \times Y^{[2]}(\hat{q})]^{[1]}$ piece of the operator show that these terms are negligible. At the worst case, the form factor value was changed in the third significant figure relative to the calculation with the $[\sigma^{[1]} \times Y^{[0]}(\hat{q})]^{[1]}$ part of the spin-current operator only. As mentioned in Sec. II, the value of the magnetic form factor at $q^2=0$ yields the magnetic moment of ${}^6\text{Li}$ ($\mu_{6\text{Li}}$).

In our calculation $F_M(0)$ yields only the spin contribution to the magnetic moment, because we only include the spin-current operator. In Table II, results of our calculations of μ_S of ${}^6\text{Li}$ for different models are given. An independent three-body calculation of $\mu_{6\text{Li}}$ for these

different models, in which the magnetic moment is calculated directly is also given in Table II. In this independent calculation, the L - S component probabilities are calculated by recoupling the three-body wave function from its Jacobi-coordinate form, and $\mu_{6\text{Li}}$ is determined using the L - S probabilities for each model.²⁸ The advantage of this approach is that the orbital (convection piece) and

TABLE II. The magnetic moment of ${}^6\text{Li}$. Experimental result, Ref. 22: $\mu_{\text{exp}} = 0.82205 \mu_N$.

Potential model	μ_S (μ_N) of this work	μ_S (μ_N) (Lehman and Parke)	μ (μ_N) (Lehman and Parke)
Simple	0.7752	0.7710	0.8328
Repulsive (0%)	0.8319	0.8283	0.8575
Repulsive (4%)	0.7972	0.7932	0.8423
Projected bound state (0%)	0.8292	0.8262	0.8566
Projected bound state (4%)	0.7946	0.7918	0.8417

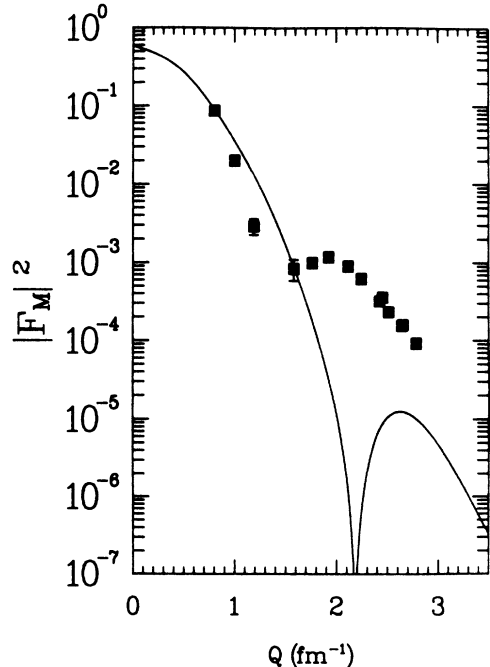


FIG. 10. The magnetic elastic form factor of ${}^6\text{Li}$ for the projected bound-state (4%) model, and the experimental data.

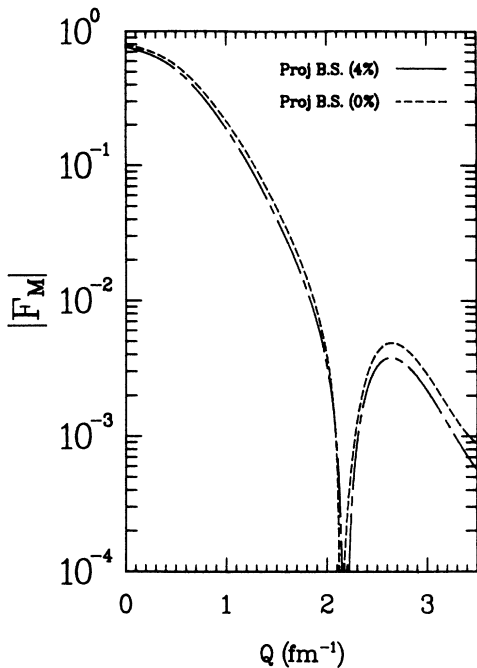


FIG. 11. The magnetic elastic form factor of ${}^6\text{Li}$ for the projected bound-state (4%), and the projected bound-state (0%) models.

spin contributions to the magnetic moment are given separately (note that $\mu = \mu_L + \mu_S$). This independent calculation serves the purpose of checking the code for the form factor.

For the production of the form factor plots, 10-Gegenbauer, 6-Gaussian, and 20-Simpson grid points were used throughout the range of q^2 values. The reason

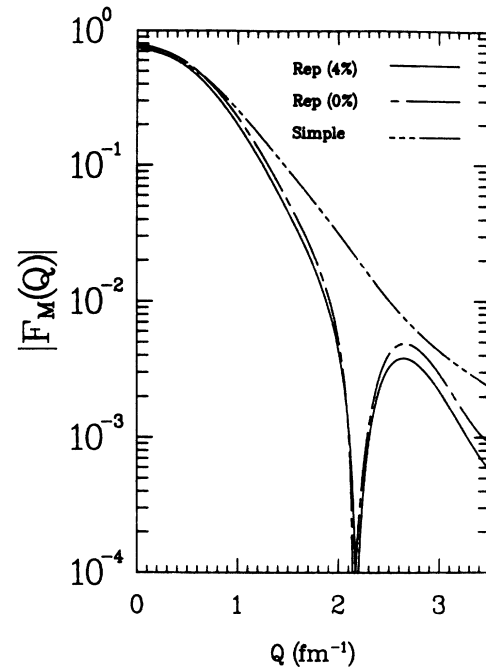


FIG. 13. The magnetic elastic form factor of ${}^6\text{Li}$ for the full-repulsive (4%), full-repulsive (0%), and the simple models.

being that the second lobe of the form factor is by 2 orders of magnitude smaller than the experimental results, and an improvement in the second or even first significant figure (which is all one gets by increasing the grid points here) would not improve the understanding of discrepancies at all; however, the cost of computations would soar if the number of grid points were significantly increased.

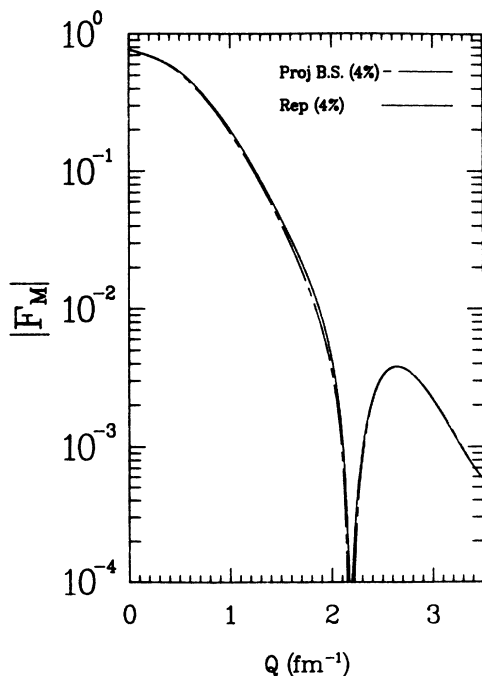


FIG. 12. The magnetic elastic form factor of ${}^6\text{Li}$ for the projected bound-state (4%) and the full-repulsive (4%) models.

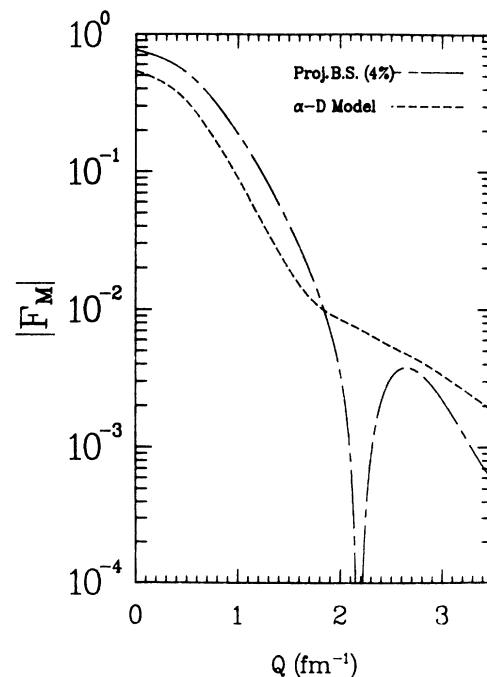


FIG. 14. The magnetic elastic form factor of ${}^6\text{Li}$ for the three-body and projected two-body (α -d) [projected bound-state (4%)] models.

Generally, all models considered here, with the exception of the simple model, exhibit a diffraction minimum between $q=2.0 \text{ fm}^{-1}$ and $q=2.5 \text{ fm}^{-1}$. The value of the form factor for higher q is lower than the experiment by approximately 2 orders of magnitude. Figures 10–14 show the form-factor calculations for all models. In Fig. 14 F_M is shown for the three-body and projected two-body (α - d) [both for the projected bound-state (4%) model] models. In this work, the magnetic form factor is compared with the experimental data of Bergstrom *et al.*¹⁰ (see Fig. 10).

IV. DISCUSSION

A. Monopole charge form factor

The following features are readily observed in an inspection of our calculations of F_{C0} for different models (see Figs. 1–5).

(1) All models except for the simple model predict a diffraction minimum about 1 fm^{-2} larger than the experiment.

(2) The 0% models are slightly larger in their values of $|F_{C0}|$ in the region of the maximum.

(3) The projected bound-state and the full-repulsive models are basically indistinguishable in terms of their prediction of the shape and magnitude of F_{C0} .

The first observation leads to one of the most important contributions of this work, namely, that the $S_{1/2}$ αN interaction is responsible for the observed diffraction minimum (note that the $P_{1/2}$ component of the αN interaction is not expected to be responsible because it is attractive and too weak in comparison with the $P_{3/2}$ component). This is most easily seen from Fig. 4 in which the results of the simple model (where the $S_{1/2}$ interaction is not included) are presented against those of the full-repulsive model. The second observation indicates that F_{C0} is sensitive to the tensor forces in the region after the minimum (Figs. 2 and 4), where the 0% models are distinctively higher than the 4% models. The third observation implies that F_{C0} is not sensitive to the particular representation of the $S_{1/2}$ interaction (Pauli's exclusion principle) in the αN system (Fig. 3).

What components of the ${}^6\text{Li}$ wave function (see the Appendix) are responsible for the diffraction minimum in $|F_{C0}|$? A detailed analysis⁴² indicates that a subtle cancellation between the terms that contain the combinations

$$(F_{1(3/2,1)}^{3/2} \times F_{1(3/2,1)}^{1/2}) \times (F_{1(3/2,1)}^{3/2} \times F_{1(3/2,1)}^{1/2})$$

and

$$G^0 \times F_{0(1/2,0)}^{1/2}$$

leads to the location of the minimum. Other contributions, e.g., $G^0 \times G^0$, tend to fill the minimum. Thus, the important role of the $F_{0(1/2,0)}^{1/2}$ component of the wave function in determining the minimum confirms our conclusion of the previous paragraph about the importance of the $S_{1/2}$ αN interaction.

A revealing picture of the distinct two- and three-body

correlations is given in Fig. 5 where, for one of the models considered [projected bound state (4%)], we present the projection of the α - d component of the three-body wave function. Here the differences seen in our solid-dash and solid curves are purely due to three-body correlations. Not only the three-body correlations are essential in getting the right magnitude for F_{C0} , but also they move the position of the diffraction minimum. An important point to note here is that for purely two-body calculations of the form factor, one should not normalize the $q^2=0$ point to unity. The exact three-body calculations show that the α - d contribution at $q^2=0$ is at most about 65%, the remaining 35% is due to the three-body α -(np) channel. Therefore, an α - d model normalized to unity at $q^2=0$ has the wrong spectroscopic factor.

The strong linear relationship between the charge radius and the binding energy (BE) given in Sec. III confirms physical intuition that larger binding should result in smaller radius. The model with the closest binding energy to the experiment is the projected bound state (4%) with a binding energy of 3.9030 MeV, bearing in mind that the Coulomb interaction is ignored in our calculation. The charge radius of 2.43 fm for this model is in agreement with the best results of Bang and Gignoux's three-body (coordinate space) calculation.¹⁹ Their calculations for Malfliet and Tjon's and for de Tourreil and Sprung's potentials yield 2.42 fm (BE=3.55 MeV) and 2.44 fm (BE=3.20 MeV), respectively. The approximately 5% discrepancy between the theory and experiment may disappear if the Coulomb interaction is included in the calculation, since the charge radius seems to be sensitive to the binding. The Russian group's three-body calculation,²⁰ where the values of the charge radius and the binding energy are both larger than the experimental measurements, is probably not that surprising because their Gaussian wave functions do not have the proper asymptotic behavior (the wave function should fall off exponentially at large distances) which manifests itself in the low q behavior of the wave function in momentum space.

Now the question arises: In the absence of a fully relativistic model, what more can be done to explain the current discrepancies? Even though we understand that in order to reproduce the experimental results we must include the missing parts of the dynamics (like three-body forces, etc.), there are a few things which can be done before one is convinced that all has been accomplished in the nonrelativistic approach. The first thing to try is to use a more sophisticated NN interaction. This has been shown to improve the cluster model results dramatically (see Jain *et al.*¹⁶). A more sophisticated NN interaction would incorporate the NN short-range repulsion and hopefully improve the binding-energy results to which the form factor seems to be sensitive at least in the low- q^2 regions. Finally, one should include the Coulomb interaction to see if the static properties can be improved.

B. Quadrupole form factor

As seen in Fig. 6, the F_{C2} form factor seems to behave exactly as expected, i.e., not much significance on the total charge form factor except for the filling of the

minimum. Figures 8 and 9 show the results for different models. What seems to dominate throughout these plots is that the projected bound-state model is higher in value throughout the q^2 values than the repulsive models, and again the 0% models are bigger than the 4% models (Fig. 7). Therefore, the F_{C2} form factor is sensitive to the particular representation of the $S_{1/2}$ interaction in the αN system (Fig. 8), especially in the $q^2 > 4 \text{ fm}^{-2}$ region. F_{C2} is also sensitive to the tensor forces (Figs. 7 and 9). As mentioned earlier numerical difficulties made the extraction of the quadrupole moment from the quadrupole form factor essentially impossible. However, we expect the wrong sign for the quadrupole-moment value since $F_{C2} > 0$ for small q in all models. This appears to be substantiated by the projected α - d model [Eq. (41)] which yields a positive value for the quadrupole moment slightly lower than that of a free deuteron. For a definite prediction of the quadrupole moment, one must resort to a direct calculation of the matrix element of the quadrupole operator.

C. Elastic magnetic form factor

An inspection of the calculated plots for F_M using our models leads us to the same conclusions that were observed for the F_{C0} form factor (Figs. 11–13). However, we must remember that in this calculation only the spin current operator is included. In Table II, the spin contribution to the magnetic moment ($\mu_{6\text{Li}}$) for different models are shown opposite to an independent calculation by Lehman and Parke.²⁸ Here, one can clearly observe that the orbital contribution to the form factor at $q=0$ is small compared to the spin part. This prompted us to include the spin current only. In addition, it is known that for the magnetic form factor of ${}^3\text{H}$, the convection-current contributions are negligible except in the region of the diffraction minimum.⁴³

Figure 10 shows that the theoretical curve falls short of the experimental data by up to 2 orders of magnitude (for $q > 2 \text{ fm}^{-1}$). Based on previous experience it is not very likely that the inclusion of the convection currents are mainly responsible for this huge discrepancy, although one must, as a first correctional step, include the convection parts of the operator in future calculations. The same remedies suggested for F_{C0} may be prescribed here for the improvement of understanding with regard to the existing discrepancies.

Our calculation, however, is rather successful in the low- q^2 region, and in particular yields magnetic moment values (see Table II) with only the spin operator in agreement with μ_S of Ref. 28 and in reasonable conformity with experiment. The only other dynamically sound calculation of the magnetic form factor performed by Kukulín *et al.*²⁰ suffers from the same discrepancy between the theory and experiment in the region of the maximum. As observed in Fig. 13, the $S_{1/2}$ interaction between α and N is again playing the major role in reproducing the diffraction minimum, and F_M is not sensitive to the representation of the $S_{1/2}$ interaction in the αN system (Fig. 12). However, the tensor forces have a definite effect in the high q region ($q > 2.5 \text{ fm}^{-1}$) after the minimum (Figs.

11 and 13).

Figure 14 shows the two-body (projected α - d model) result and the full three-body calculation for the magnetic form factor. As is clear from the figure, for high q^2 values the α - d model fails to reproduce the minimum. In spite of the fact that only the s -wave piece of the α - d momentum distribution is included, one can conclude that three-body correlations are even more pronounced in the case of the transverse elastic form factor for getting the right shape of the F_M form factor.

V. CONCLUSION

The present work that uses the LRG three-body wave function to determine the elastic electromagnetic form factors of ${}^6\text{Li}$, confirms that the LRG model is successful in explaining the low- q (momentum transfer) behavior of the electromagnetic form factors, which lie within the realm of the validity of the model. It is surprising that even for higher- q values, the model can predict the general shape properly and provides a qualitative explanation of the physics of the form factors. This shows that it is possible to do a consistent nonrelativistic three-body calculation of the elastic electromagnetic form factors of ${}^6\text{Li}$, based on the low-energy parametrization of the underlying two-body interactions of the constituent particles. Once these parameters are set, no further parametrization occurs and calculations of physical observables are direct predictions of the three-body model.

Basically the static properties of ${}^6\text{Li}$, extracted from the form factors (charge radius, magnetic moment), are predicted within a few percent with the exception of the quadrupole moment for which a separate calculation should be done to circumvent numerical problems. A study of the shape of the form factors shows the importance of the $S_{1/2}$ interaction in the αN system for the prediction of the diffraction minima of the form factors. All the form factors (except for F_{C2} in the high- q region) are insensitive to the particular representations of the $S_{1/2}$ interaction in the αN system. On the other hand, the tensor forces are felt by all the form factors considered here, lowering the form factor values at higher- q values (generally beyond the diffraction minimum).

The following steps might be considered for refinement of the model: (1) Employ a more sophisticated NN interaction to incorporate short-range repulsion. (2) Include the Coulomb interaction to further improve the binding energy and thus the charge radii and to assure that the low- q^2 discrepancies are purely a binding effect; all this in the elastic longitudinal form factors. (3) For the elastic magnetic form factor, inclusion of the convection currents is the natural extension of the work done here.

ACKNOWLEDGMENTS

A.E. gratefully acknowledges several useful discussions with and computational assistance from Leonard Maximon. This article is based in part on the Ph.D. dissertation of the first author (Ref. 42). The work of the authors was supported in part by the U.S. Department of Energy under Grant No. DE-FG05-86ER40270. Computer time for this work was supported by the Florida State Univer-

sity Supercomputer Computations Research Institute which is partially funded by the U.S. Department of Energy through Contract No. DE-FC05-85ER250000.

APPENDIX

This appendix explicitly defines the form of the three-body wave function used in this paper. The Jacobi-coordinate \mathbf{s} is used to define the relative position of the proton (1) with respect to the neutron (2), while $\boldsymbol{\rho}$ gives the coordinate of the α particle (3), relative to the (n,p) pair, both \mathbf{s} and $\boldsymbol{\rho}$ are defined in the center of mass of the three-body system, and are related to the center-of-mass coordinates of the three particles by

$$\mathbf{r}_1 = \frac{\mathbf{s}}{2} - \frac{2\boldsymbol{\rho}}{3}, \quad (\text{A1})$$

$$\mathbf{r}_2 = -\frac{\mathbf{s}}{2} - \frac{2\boldsymbol{\rho}}{3}, \quad (\text{A2})$$

$$\mathbf{r}_3 = \frac{\boldsymbol{\rho}}{3}. \quad (\text{A3})$$

In momentum space, the conjugate Jacobi momenta are used, where \mathbf{k}_{ij} denotes the relative momentum of the i th and j th particles, while \mathbf{p}_k represents the relative momentum of the k th particle with respect to the center of mass of the other two. In terms of $\mathbf{k}_{12} \equiv \mathbf{k}$, $\mathbf{p}_3 \equiv \mathbf{p}$, the permuted sets are given by

$$\mathbf{k}_{23} = -\frac{4}{3}\mathbf{k} + \frac{3}{5}\mathbf{p}, \quad (\text{A4})$$

$$\mathbf{p}_1 = -\mathbf{k} - \frac{1}{2}\mathbf{p}, \quad (\text{A5})$$

$$\mathbf{k}_{31} = -\frac{4}{3}\mathbf{k} - \frac{3}{5}\mathbf{p}, \quad (\text{A6})$$

$$\mathbf{p}_2 = \mathbf{k} - \frac{1}{2}\mathbf{p}. \quad (\text{A7})$$

The wave function of ${}^6\text{Li}$ as defined by LRG (Ref. 8) can then be written as

$$\Psi_M^{[1]}(\mathbf{k}_{12}, \mathbf{p}_3) = \frac{4\pi}{K^2 + k_{12}^2 + \frac{3p_3^2}{8}} \left[\lambda_1 \sum_{\substack{l,l'=0 \\ l,l' \neq 1}}^2 g_l^l(k_{12}) G^{l'}(p_3) \{ [Y^{[l]}(\hat{\mathbf{k}}_{12}) \times \chi^{[1]}(12)]^{[1]} \times Y^{[l']}(\hat{\mathbf{p}}_3) \}_M^{[1]} \right. \\ \left. + \frac{5}{8} \sum_{J=1/2}^{3/2} \sum_{J'=|1-J|}^{1+J} \sum_{l'=J'-1/2}^{J'+1/2} P^{l+l'} \Lambda_l^J \right. \\ \left. \times \{ h_l^J(k_{23}) F_{l'(J)}^{J'}(p_1) [\mathcal{Y}_{l(1/2)}^{[J]}(\hat{\mathbf{k}}_{23}, 2) \times \mathcal{Y}_{l'(1/2)}^{[J']}(\hat{\mathbf{p}}_1, 1)]_M^{[1]} \right. \\ \left. + (-1)^l h_l^J(k_{31}) F_{l'(J)}^{J'}(p_2) \right. \\ \left. \times [\mathcal{Y}_{l(1/2)}^{[J]}(\hat{\mathbf{k}}_{31}, 1) \times \mathcal{Y}_{l'(1/2)}^{[J']}(\hat{\mathbf{p}}_2, 2)]_M^{[1]} \} \right],$$

where

$$\mathcal{Y}_{l(1/2)}^{[J]}(\hat{\mathbf{k}}, 2) = \sum_{\mu\eta} \langle l\mu \frac{1}{2}\eta | JM \rangle Y_\mu^{[1]}(\hat{\mathbf{k}}) \chi_\eta^{[1/2]}(2)$$

and

$$P^L = \frac{[1 + (-1)^L]}{2}.$$

The spectator function $G^l(p)$ is the l -wave momentum distribution amplitude of the α -particle relative to the center of mass of the two nucleons, and $F_{l'(J)}^{J'}(p)$ gives the total-angular-momentum J' -orbital angular-momentum l' component of the momentum distribution amplitude of a nucleon relative to the center of mass of an α - N pair in the Jl state of their interaction. It should be mentioned that the isospin function is suppressed in the above ex-

pression, and the wave function is symmetric under the exchange of particles 1 and 2. $g_l^l(k)$ and $h_l^J(k)$ are NN and αN interaction form factors, respectively, and are analytically represented by

$$g_l^l(k) = \frac{(l^{1/2}k)^l}{[k^2 + (\beta_l^1)^2]^{(l+2)/2}},$$

$$h_l^J(k) = \frac{k^l}{[k^2 + (\beta_l^J)^2]^{(l+1)}},$$

where the β_l^J 's are the inverse range parameters for the potential.

λ_1 and Λ_l^J are the strength parameters of the potentials. For a more complete description of the potentials and wave function components see LRG.⁸

*Current address: School of Physical Sciences, The Flinders University of South Australia, Bedford Park, South Australia 5042.

¹D. R. Lehman and M. Rajan, Phys. Rev. C **25**, 2743 (1982); W. C. Parke and D. R. Lehman, *ibid.* **29**, 2319 (1984); C. T.

Christou, C. J. Seftor, W. J. Briscoe, W. C. Parke, and D. R. Lehman, *ibid.* **31**, 250 (1985); R. Ent, H. P. Blok, J. F. A. van Heinen, G. van der Steenhoven, J. F. J. van den Brand, J. W. A. den Herder, E. Jans, P. H. M. Keizer, L. Lapikas, E. N. M. Quint, P. K. A. deWitt Huberts, B. L. Berman, W. J.

- Briscoe, C. T. Christou, D. R. Lehman, B. E. Norum, and A. Saha, *Phys. Rev. Lett.* **57**, 2367 (1986).
- ²M. Rai, D. R. Lehman, and A. Ghovanlou, *Phys. Lett.* **59B**, 327 (1975).
- ³W. C. Parke, A. Ghovanlou, C. T. Noguchi, M. Rajan, and D. R. Lehman, *Phys. Lett.* **74B**, 158 (1978).
- ⁴C. T. Christou, D. R. Lehman, and W. C. Parke, *Phys. Rev. C* **37**, 445 (1988); **37**, 458 (1988); **37**, 477 (1988).
- ⁵P. E. Shanley, *Phys. Rev. Lett.* **21**, 627 (1968); *Phys. Rev.* **187**, 1328 (1969).
- ⁶Y. Koike, *Prog. Theor. Phys.* **55**, 2016 (1976); **59**, 87 (1978); *Nucl. Phys.* **A301**, 411 (1978); **A337**, 23 (1980).
- ⁷B. Charnomardic, C. Fayard, and G. H. Lamot, *Phys. Rev. C* **15**, 864 (1977).
- ⁸D. R. Lehman, M. Rai, and A. Ghovanlou, *Phys. Rev. C* **17**, 744 (1978).
- ⁹G. C. Li, I. Sick, R. R. Whitney, and M. R. Yearian, *Nucl. Phys.* **A162**, 583 (1971).
- ¹⁰J. C. Bergstrom, S. B. Kowalski, and R. Neuhausen, *Phys. Rev. C* **25**, 1156 (1982).
- ¹¹Gerald L. Payne and B. P. Nigam, *Phys. Rev. C* **21**, 1177 (1980).
- ¹²M. Bouten, M. C. Bouten, and P. van Leuven, *Phys. Lett.* **26B**, 191 (1968).
- ¹³H. Kanada, T. Kaneko, and Y. C. Tang, *Nucl. Phys.* **A389**, 285 (1982).
- ¹⁴J. C. Bergstrom, *Nucl. Phys.* **A327**, 458 (1979).
- ¹⁵J. V. Noble, *Phys. Rev. C* **9**, 1209 (1974).
- ¹⁶A. K. Jain and N. Sarma, *Phys. Lett.* **33B**, 271 (1970).
- ¹⁷A. C. Merchant and N. Rowley, *Phys. Lett.* **150B**, 35 (1985); S. Sack, L. C. Biedenharn, and G. Breit, *Phys. Rev.* **93**, 321 (1954).
- ¹⁸T. Mertelmeir and H. M. Hofmann, *Nucl. Phys.* **A459**, 387 (1986); H. M. Hofmann, T. Mertelmeir, and D. Sachsenweger, *Charge Form Factors for ${}^6\text{Li}$ and ${}^7\text{Li}$ in the Cluster Model*, in *Book of Contributions, Eleventh International IUPAP Conference on Few Body Systems in Particle and Nuclear Physics*, Tohoku, 1986, edited by T. Sasakawa, K. Nisimura, S. Oryu, and S. Ishikawa [Suppl. Res. Rep. Lab. Nucl. Sci. **19**, 258 (1986)].
- ¹⁹J. Bang and C. Gignoux, *Nucl. Phys.* **A313**, 119 (1979).
- ²⁰V. I. Kukulin, V. K. Krasnopol'sky, and V. I. Voronchev, and P. B. Sazanov, *Nucl. Phys.* **A417**, 128 (1984); V. I. Kukulin, V. M. Krasnopol'sky, V. T. Voronchev, and P. B. Sazanov, *ibid.* **A453**, 365 (1986).
- ²¹F. Ajzenberg-Selove, *Nucl. Phys.* **A413**, 1 (1984).
- ²²A. Malfliet and J. A. Tjon, *Nucl. Phys.* **A127**, 161 (1962).
- ²³R. de Tourreil, B. Rouben, and D. W. L. Sprung, *Nucl. Phys.* **A242**, 445 (1975); **A201**, 193 (1973).
- ²⁴G. R. Satchler, L. W. Owen, A. J. Elwyn, G. L. Morgan, and R. L. Walther, *Nucl. Phys.* **A112**, 1 (1986).
- ²⁵V. T. Voronchev, V. M. Krasnopol'sky, and V. I. Kukulin, *J. Phys. G* **8**, 649 (1982).
- ²⁶V. T. Voronchev, V. M. Krasnopol'sky, V. I. Kukulin, and P. B. Sazanov, *J. Phys. G* **8**, 667 (1982).
- ²⁷V. M. Krasnopol'ski, V. I. Kukulin, P. B. Sazanov, and V. T. Voronchev, *Phys. Lett.* **121B**, 96 (1983).
- ²⁸D. R. Lehman and W. C. Parke, *Few Body Systems* **1**, 193 (1986).
- ²⁹D. R. Lehman, *Phys. Rev.* **25**, 3146 (1982); V. M. Krasnopol'ski and V. I. Kukulin, *Yad. Fiz.* **20**, 883 (1974) [*Sov. J. Nucl. Phys.* **20**, 470 (1975)].
- ³⁰N. K. Glendenning and G. Kramer, *Phys. Rev.* **126**, 2159 (1962).
- ³¹M. Gourdin, *Nuovo Cimento* **28**, 533 (1963).
- ³²Loyal Durand, *Phys. Rev.* **123**, 1393 (1961).
- ³³V. Glaser and B. Jaksic, *Nuovo Cimento* **5**, 1197 (1957).
- ³⁴U. Fano and G. Racah, *Irreducible Tensorial Sets* (Academic, New York, 1959); M. Danos, *Ann. Phys. (N.Y.)* **63**, 319 (1971); D. R. Lehman and J. S. O'Connell, *Graphical Recoupling of Angular Momenta*, Natl. Bur. Stand. (U.S.) Monogr. **136** (U.S. GPO, Washington, D.C., 1973).
- ³⁵J. L. Friar, *Phys. Rev. C* **27**, 2078 (1983).
- ³⁶J. L. Friar, *Ann. Phys.* **104**, 380 (1977).
- ³⁷M. Rajan, Ph.D. dissertation, The George Washington University, 1976 (unpublished).
- ³⁸W. C. Parke and D. R. Lehman (unpublished).
- ³⁹G. Höhler, E. Pieterinen, I. Sabba-Stefanescu, F. Borkowski, G. G. Simon, V. H. Walther, and R. D. Wendling, *Nucl. Phys.* **B114**, 505 (1976).
- ⁴⁰R. F. Frosch, J. S. McCarthy, R. E. Rand, and M. R. Yearian, *Phys. Rev.* **160**, 874 (1967).
- ⁴¹J. L. Friar, private communication.
- ⁴²A. Eskandarian, Ph.D. dissertation, The George Washington University, 1987 (unpublished).
- ⁴³B. Goulard, private communication.